

## Article

# Efficient Uncertainty Analysis of External Heat Flux of Solar Radiation with External Heat Flux Expansion for Spacecraft Thermal Design

Xiaoyi Fu, Lei Liang \*, Wenlai Ma, Hutao Cui and Yang Zhao

School of Astronautics, Harbin Institute of Technology, Harbin 150001, China; 19b918083@stu.hit.edu.cn (X.F.)

\* Correspondence: lianglei@hit.edu.cn

**Abstract:** Designing spacecraft involves a careful equilibrium to avoid overengineering or underdesigning, which underscores the importance of employing thermal uncertainty analysis. A key part of this analysis is modeling thermal conditions, but this is often a computationally heavy process. This is largely because ray-tracing calculations require determining the external heat flux of solar radiation across different operating conditions. Ray emission varies across conditions, which can lead to inefficient resource use in uncertainty calculations. Our study aims to address this by introducing a new approach to calculating the external heat flux of solar radiation that is better suited for uncertainty analysis than previous approaches. Our formula only requires ray tracing to be performed for one condition rather than for every condition. The other conditions are handled by simple matrix budgeting, negating the need for complicated ray tracing. In the aforementioned analytical procedure, certain matrices demonstrate sparsity properties. By exploiting this characteristic, optimization computations can be executed by utilizing sparse matrix algorithms. We tested this new formula, which we call the external heat flux expansion (EHFE) formula, on a specific spacecraft and compared the results with those obtained using the traditional method. Our findings suggest that the EHFE formula is ideal for calculating uncertainty. It significantly improves computational efficiency while maintaining accuracy. The formula is also user-adjustable, allowing the accuracy of uncertainty calculation results of the external heat flux of solar radiation to be fine-tuned by changing the value of the cutoff factor. This work establishes an essential theoretical framework pivotal to addressing inherent uncertainties in the thermal design of upcoming deep-space exploration spacecraft, solar observatory satellites, and space solar power stations.

**Keywords:** spacecraft; uncertainty thermal analysis; ray tracing; solar radiation external heat flux; external heat flux expansion; sparse matrix algorithms



**Citation:** Fu, X.; Liang, L.; Ma, W.; Cui, H.; Zhao, Y. Efficient Uncertainty Analysis of External Heat Flux of Solar Radiation with External Heat Flux Expansion for Spacecraft Thermal Design. *Aerospace* **2023**, *10*, 672. <https://doi.org/10.3390/aerospace10080672>

Academic Editors: Reinaldo R. Souza, Ana Moita, João Ribeiro and Rui A. Lima

Received: 7 July 2023  
Revised: 26 July 2023  
Accepted: 26 July 2023  
Published: 28 July 2023



**Copyright:** © 2023 by the authors. Licensee MDPI, Basel, Switzerland. This article is an open access article distributed under the terms and conditions of the Creative Commons Attribution (CC BY) license (<https://creativecommons.org/licenses/by/4.0/>).

## 1. Introduction

Spacecraft function within an exceedingly demanding and largely variable environment, where meticulously regulating temperature is crucial for maintaining and operating onboard instruments and systems. Consequently, the design and operation of extraterrestrial vehicles has persistently emphasized spacecraft thermal analysis. Nevertheless, the inherent complexity of this domain renders it nearly impossible to devise entirely deterministic models of thermal behavior. Thermal analysts are compelled to tackle and merge diverse sources of uncertainty as an alternative, thereby making uncertainty analysis an indispensable facet of spacecraft thermal design.

Uncertainty analysis in spacecraft thermal design allows us to estimate the potential range of outcomes and assess the risks associated with different thermal management strategies. A thermal design that has not undergone rigorous uncertainty analysis may perform well under nominal conditions but fail under slightly off-nominal conditions, which are inevitable due to the dynamic and unpredictable nature of the space environment. The repercussions of such failures could vary from minor instrument performance

degradation to severe system malfunction, culminating, in the worst-case scenario, in mission failure [1,2].

The seminal research conducted by Ishimoto and Bevans [3], Howell [4], and Thunnissen [5] underscores that the principal aim of uncertainty analysis is developing a superior methodology for computing design margins. The fundamental notion of uncertainty analysis involves model uncertainty being meticulously accounted for before the 'development of the model and subsequently propagated through the model, thereby quantifying the uncertainty inherent in the' output of the model. Its ability to furnish design margins tailored to specific instances curtails overdesign and mitigates the challenges associated with underdesign, demonstrating its superiority over conventional techniques.

With increasing mission complexity and decreasing budgets, the importance of uncertainty analysis in spacecraft thermal design cannot be overlooked. With the advent of more sophisticated spacecraft and payloads, as well as increasingly ambitious types and locales of missions, thermal environments have become progressively more difficult to predict and control. A comprehensive understanding of the uncertainties inherent in thermal analysis and design is, therefore, critical for the continued advancement of space exploration.

Presently, the Monte Carlo (MC) method is the principal technique employed for thermal uncertainty analysis calculations in spacecraft. Nonetheless, Monte Carlo simulations may be computationally burdensome, requiring many runs to attain statistically significant outcomes. This process can be resource-draining and time-intensive, particularly for intricate thermal models. Extensive research has been undertaken to strike a balance between the precision and speed of thermal uncertainty analysis algorithms. Thunnissen [6] used subset simulation for transient thermal uncertainty analysis during the cruise phase of a Mars spacecraft. The tail probability distribution function for the maximum temperature of essential components was ascertained, illustrating congruity with MC results and a substantial reduction in computational effort. Gómez-San-Juan [7] enhanced statistical error analysis and introduced a one-dimensional generalized statistical error analysis method. The input uncertainty variables of the method exhibited arbitrary distributions. The non-linear relationship between node temperature and uncertainty variables was considered. It has a similar computation time as statistical error analysis and a similar accuracy as the MC method. Xiong Yan [8] employed a radial basis function neural network and an enhanced thinking evolutionary algorithm to approximate thermophysical models for conventional spacecraft, significantly enhancing the analysis rate of steady-state thermal uncertainty analysis within the trained neural network. Kato [9] implemented a simulator with Gaussian process regression and a minimum absolute shrinkage selection operator for satellite thermal uncertainty analysis, decreasing the uncertainty quantification cost. Similarly, the Kriging model [10–13], radial basis function [14], artificial neural network [15,16], support vector regression [17], and response surface method [18] served as surrogate models replacing thermal analysis models of spacecraft. Thermal uncertainty analysis was conducted on the surrogate models to boost computational efficiency. Nevertheless, the original thermal analysis model of spacecraft required comprehensive sampling and several computations to obtain an accurate surrogate model. This can be challenging in high-dimensional or complex parameter spaces.

The aforementioned methods enhance computational efficiency of thermal uncertainty analysis under mathematical methodologies. In this paper, a native thermal analysis model of spacecraft is optimized to improve the computational efficiency of thermal uncertainty analysis. Radiation model calculation and thermal model calculation are the two primary steps in determining the temperature field of spacecraft when computing the native thermal analysis model of the spacecraft. The literature [7] indicates that the time required for radiation model calculations significantly exceeds that required for thermal model calculations. Radiation Monte Carlo ray-tracing computation is the most time-intensive task. Radiation Monte Carlo ray-tracing computations are primarily intricate procedures such as determining ray emission points, generating emission directions, and identifying multiple intersections of rays with spacecraft. This process involves tracing the

trajectories of millions or even billions of individual rays. The simulation of external heat flux absorbed by a spacecraft's surface is the most time-consuming task.

The external heat flux of solar radiation is the most substantial component of the external heat flux absorbed by the surfaces of spacecraft. It has the greatest impact on temperatures across all spacecraft components and directly dictates the equilibrium temperature level of spacecraft. Thermal uncertainty analysis requires multiple computations of the external heat flux of solar radiation via the Monte Carlo ray-tracing algorithm. This is one of the primary contributors to the considerable computational expense associated with thermal uncertainty analysis.

When performing thermal uncertainty analysis for spacecraft, random numbers are used to generate multiple samples of operating thermal property parameters. The computation of the external heat flux of solar radiation is executed independently for each operating condition. This procedure is repeated multiple times to emit rays for the calculation of external heat flux of solar radiation, resulting in a substantial waste of rays and critically escalating the computational duration.

In an effort to address ray wastage during the calculation of uncertainty in the external heat flux of solar radiation, this study aims to comprehensively expand the traditional equation used for said calculation. The uncertainty variables of the equation are sufficiently isolated, thereby developing a new formula specifically for the calculation of the external heat flux of solar radiation. Drawing on this newly devised formula for the external heat flux uncertainty calculation, ray emission is required for only the initial operating condition for ray tracing to calculate the external heat flux of solar radiation. However, an additional EHFE matrix must be generated during this process, facilitating applications to other conditions of uncertainty analysis. Thermal uncertainty analysis of other operating conditions involves substituting new samples of thermal property parameters into the matrix for computation. This innovative formula is particularly suited to the uncertainty analysis of the external heat flux of solar radiation. This circumvents the need to emit rays for each operating condition and perform ray tracing to calculate the external heat flux, instead substituting a simple matrix operation for the originally complex ray-tracing calculation process. This methodology for calculating the uncertainty of external heat flux can effectively decrease computation time while maintaining a certain degree of computational accuracy.

This paper is structured as follows: in Section 2, the external heat flux ray-tracing approach and the conventional calculation algorithm for the external heat flux of solar radiation are introduced. In Section 3, the solar radiation EHFE formulation is introduced, the process of its expansion to develop a new formula is described in detail, and how to use this formula to perform uncertainty analysis for external heat flux is explained. In Section 4, the composition and various uncertainty analysis calculation parameters of a spacecraft are presented as an example. In Section 5, the obtained uncertainty analysis results for the spacecraft's external heat flux of solar radiation are discussed and analyzed. Finally, conclusions are drawn in Section 6.

## 2. External Heat Flux of Solar Radiation

The external heat flux of solar radiation can be sorted into two distinct categories: the external heat flux of direct and of indirect solar radiation. In spacecraft thermal design, the external heat flux stemming from direct solar radiation consists of parallel rays. In contrast, external heat flux of indirect solar radiation is formed by diffuse radiation, which originates from the reflection of the aforementioned rays off a diffusely reflective surface.

The following three ray-tracing methods can calculate the external heat flux: the collision method, the path length method, and the path length method with the introduction of a cutoff factor [19]. In this paper, the path length method with the introduction of a cutoff factor is used to solve for the external heat flux of solar radiation. The cutoff factor is set to 0.1.

### 2.1. External Heat Flux of Direct Solar Radiation

The sun shines on the Earth and creates a shadow zone behind the Earth. When a spacecraft is orbiting in the Earth's shadow zone, the direct solar radiation on the spacecraft is zero. Even if the spacecraft is fully in the illuminated region, certain surface elements are not exposed to direct solar radiation because they are blocked by other surface elements. Therefore, when calculating the external heat flux of direct solar radiation absorbed by the surface elements of the surface, the first step is to make a shading judgment and an obscuring judgment.

**Shading judgment:** If the ray emitted from the spacecraft surface element intersects with the Earth's surface, this ray is in the shadow region. If there is no intersection, this ray is in the illuminated area.

**Obscuring judgment:** If the ray emitted from the spacecraft surface element intersects with another surface of the spacecraft, this ray is obscured by the surface where the intersection is located. If the ray does not intersect with any other face element of the spacecraft, the ray is not obscured.

The unshaded face element in the illuminated area is truly exposed to direct solar radiation only on the side where the angle between the normal vector and the solar ray vector is greater than  $90^\circ$ .

The approach adopted in this study leverages the reverse Monte Carlo (RMC) model to emit random rays from spacecraft surface elements. Rays pertaining to direct solar radiation are parallel rays, which are distinct from the random rays emitted during Earth albedo radiation calculations, Earth infrared radiation, and indirect solar radiation. In resolving the external heat flux of direct solar radiation, the direction of the random rays released from the surface element aligns with that of the inverse vector of the solar ray vector.

If the angle between the normal vector of the face element  $E_i$  and the sun ray vector is greater than  $90^\circ$ , the face element  $E_i$  emits a total of  $N_{sd}$  random rays. The path length method with the introduction of a cutoff factor is used for ray tracing. There are  $N_{sa}$  rays in the illuminated area that are not obscured. Then, the external heat flux of direct solar radiation absorbed by the surface element  $E_i$  is calculated as follows:

$$q_{sd}^i = \frac{1}{N_{sd}} \sum_{j=1}^{N_{sa}} S \times |\cos \theta_{E_i}| \times \alpha_{E_i}^s \quad (1)$$

where  $S$  is the solar constant,  $\theta$  is the angle between the normal vector of the face element  $E_i$  and the solar ray vector, and  $\alpha_{E_i}^s$  is the solar absorption rate of the surface element  $E_i$  [20–25].

### 2.2. External Heat Flux of Indirect Solar Radiation

The RMC method is a general approach for computing the external heat flux of indirect solar radiation absorbed by surface elements.  $N$  rays are emitted from the target surface element and ray tracing is conducted on them. The  $N$ -ray results are statistically analyzed to determine the external heat flux of indirect solar radiation for the target surface element. The RMC simulation for a single ray proceeds as follows:

- (1) Reference coordinate systems, such as body, orbit, and geocentric inertial coordinate systems, are established and orbit parameters are provided;
- (2) A thermal–physical model of the spacecraft structure is constructed, a grid of thermal analysis surface elements is partitioned, and the surface equation and radiation characteristics for each thermal analysis surface element are determined;
- (3) A target surface element of the spacecraft emits a random ray;
- (4) The intersection of the ray with the surface element of the system (spacecraft and radiation source) is calculated and the method for further tracking the ray is determined according to the ray-tracing technique;

- (5) If the ray is absorbed by the radiation source's surface, the external heat flux absorbed by the ray on the target surface element's surface is accounted for using the reverse process.

In this paper, random rays are emitted from the spacecraft's target surface elements based on the RMC principle, and the path length method with the introduction of a cutoff factor is used for ray tracing. The  $N_{si}$  rays emitted from the spacecraft's face elements  $E_i$  are tracked. If there are  $N_{si}^A$  rays reaching the surface element irradiated by direct solar radiation, the external heat flux of indirect solar radiation absorbed by the surface element  $E_i$  is calculated as follows:

$$q_{si}^i = \frac{1}{N_{si}} \sum_{j=1}^{N_{si}^A} \frac{q_{sd,j} \times (1 - \alpha^{s,j})}{\alpha^{s,j}} \times \alpha_{E_i}^s \times K_{si}^j \quad (2)$$

where  $q_{sd,j}$  is the external heat flux of direct solar radiation absorbed by the face element where the  $j$ th ray eventually arrives, and  $\alpha^{s,j}$  is the solar absorption rate corresponding to the face element where the  $j$ th ray eventually arrives [20–25].

$$K_{si}^j = \begin{cases} 1 & k = 0 \\ \prod_{\tau=1}^k (1 - \alpha_{E_\tau}^s) & k \neq 0 \end{cases} \quad (3)$$

where  $k$  is the number of ray reflections.

In summary, the external heat flux of solar radiation absorbed by face element  $E_i$  is  $q_s^i = q_{sd}^i + q_{si}^i$ .

### 3. External Heat Flux of Solar Radiation Uncertainty Calculation

To conduct thermal uncertainty analysis of the spacecraft, the MC method is employed to generate  $N$  operational conditions. Since calculating external heat flux of solar radiation necessitates multiple ray-tracing operations and the application of ray-judgment intersection algorithms, the duration required for radiation model computation exceeds that required for thermal model computation. During uncertainty analysis, it is necessary to run the external heat flux of solar radiation calculation model repeatedly and extensively and make several complex ray-tracing and intersection judgments. Furthermore, in these  $N$  conditions, rays emitted under each condition are autonomous and noninteracting. This implies that the rays from a prior operational condition are not utilized in the subsequent one, leading to inadequate emitted ray utilization. The uncertainty variables involved in calculating the external heat flux of solar radiation include the solar absorptivity and reflectivity of the surface coating of the spacecraft. In this study, the conventional equation for calculating the external heat flux of solar radiation is thoroughly expanded, ensuring adequate separation of uncertainty variables within the equation to develop a new formula for this calculation. Ultimately, this new formula is employed to perform uncertainty analysis of the external heat flux of solar radiation absorbed by the spacecraft. According to Figure 1, the new formula is calculated as a simple matrix operation, avoiding the complex ray-tracing process.

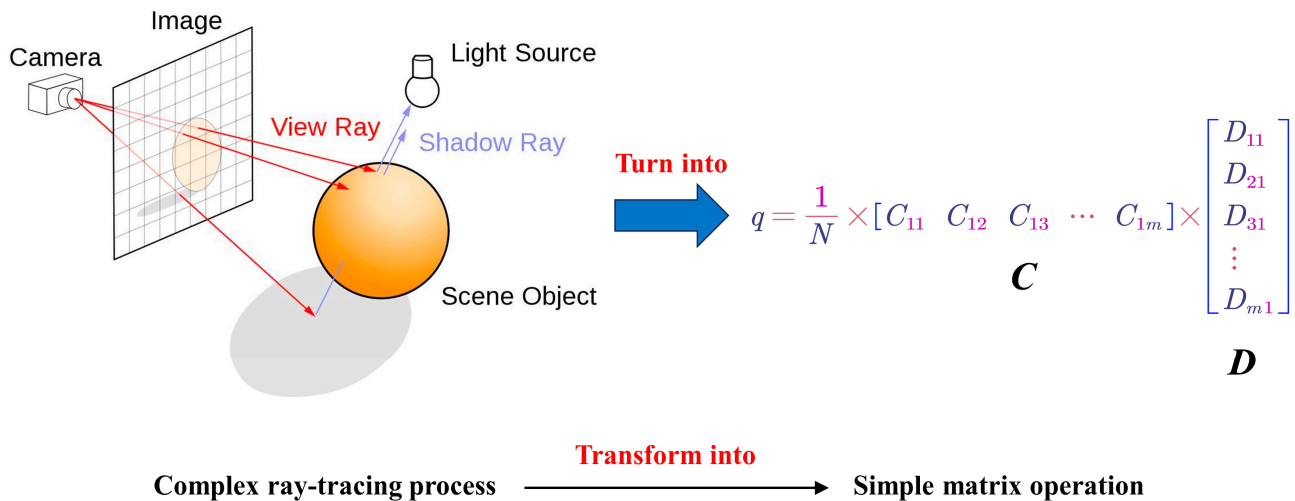


Figure 1. Comparison of the calculations between traditional and new methods.

3.1. Direct Solar Radiation Uncertainty Analysis with EHFE

3.1.1. Direct Solar Radiation EHFE Equation

The reflection phenomenon of rays is not involved in calculating the external heat flux of direct solar radiation. Therefore, the uncertainty variables in Equation (1) can be completely and directly separated out. The separated equation is as follows:

$$q_{sd-old}^i = \frac{N_{sa}}{N_{sd}} \times C_{sd} \times D_{sd} \tag{4}$$

where  $C_{sd} = S \times |\cos \theta_{E_i}|$ ,  $D_{sd} = \alpha_{E_i}^s$ .

3.1.2. External Heat Flux of Direct Solar Radiation Uncertainty Analysis

Before performing the uncertainty analysis, the external heat flux of direct solar radiation absorbed by the primary target surface element must be solved by using the RMC ray-tracing algorithm. The  $N_{sa}$  and  $N_{sd}$  values obtained during the solving process must be recorded. Later, when performing uncertainty analysis, ray tracing is no longer performed for each operating condition, as in the traditional method. Instead, a sample of coated solar absorbance is generated using random numbers.  $D_{sd}$  is updated to  $D_{sd}^1$  using the above sample. Finally, the updated element is substituted into Equation (5) to solve for the external heat flux of direct solar radiation considering the uncertainty.

$$q_{sd-new}^i = \frac{N_{sa}}{N_{sd}} \times C_{sd} \times D_{sd}^1 \tag{5}$$

The comparison of two processes for calculating the external heat flux of direct solar radiation taking into account parameter uncertainties is shown in Figure 2.

The main steps of the conventional method for solving the external heat flux of direct solar radiation considering uncertainties are as follows:

- (1) Generation of samples of solar absorbance of all face elements of the spacecraft using random numbers;
- (2) RMC for ray-tracing, ray-shading, and obscuring judgments, and solving for external heat flux of direct solar radiation;
- (3) Repeating (1) and (2) to generate multiple  $q_{sd}^i$  samples for statistics.

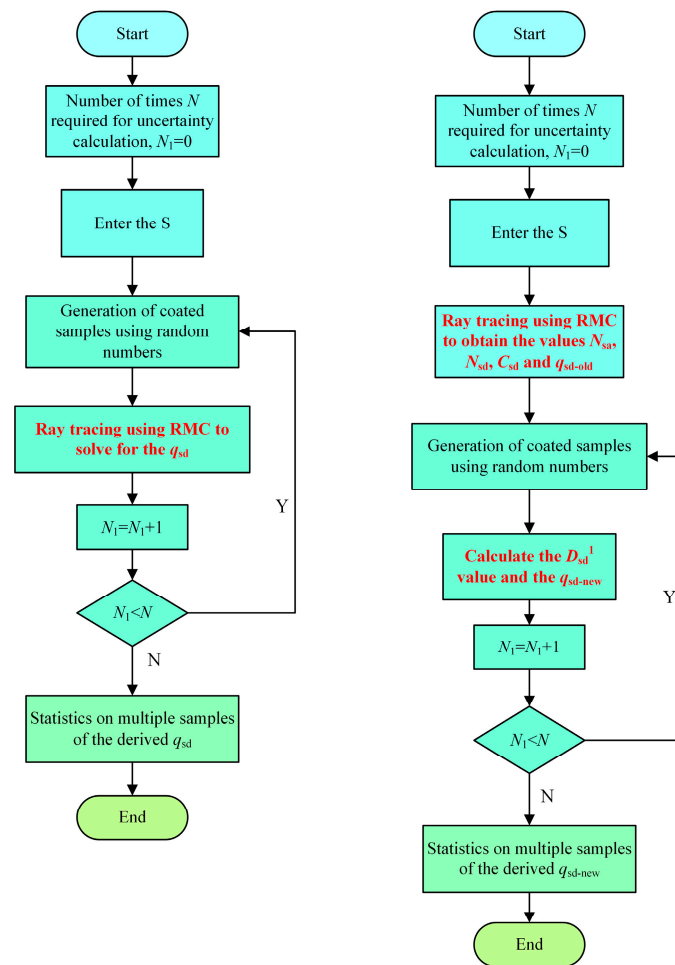


**Figure 2.** Comparison of two processes for solving external heat flux of direct solar radiation considering parameter uncertainty, left (conventional) and right (based on EHFE equation).

The main steps for solving the external heat flux of direct solar radiation considering uncertainty using the EHFE formula are as follows:

- (1) Ray tracing using RMC to solve for the initial working conditions of the external heat flux of direct solar radiation and recording the values of  $N_{sa}$  and  $N_{sd}$ ;
- (2) Generation of samples of solar absorptance of all face elements of the spacecraft using random numbers;
- (3) Updating of element  $D_{sd}$  to generate element  $D_{sd}^1$  based on samples of solar absorptance corresponding to the new working condition;
- (4) Using Equation (5) to solve for  $q_{sd-new}^i$ ;
- (5) Repeating (2)–(4) to generate multiple  $q_{sd-new}^i$  samples for statistics.

In summary, the original solution to the external heat flux of direct solar radiation equation is expanded. Separating the uncertainty variables in the equation, we construct a new formula  $q_{sd-old}^i = \frac{N_{sa}}{N_{sd}} \times C_{sd} \times D_{sd}$  for calculating the external heat flux of direct solar radiation. The thermal uncertainty analysis based on this equation is ray-traced for the initial operating conditions only. Other operating conditions do not require ray emission for a complex ray-tracing process. For other operating conditions, the calculation is performed by substituting the new solar absorptance sample into the corresponding element position of  $q_{sd-new}^i = \frac{N_{sa}}{N_{sd}} \times C_{sd} \times D_{sd}^1$ . EHFE replaces traditional ray-tracing methods. It can effectively reduce the cost of thermal uncertainty analysis calculations.

### 3.2. Indirect Solar Radiation Uncertainty Analysis with EHFE

#### 3.2.1. Indirect Solar Radiation EHFE Equation

To completely separate the coating’s solar absorbance and reflectance, Equation (2) is further expanded as in Equation (6). The first term of the equation represents the ray directly reaching the spacecraft surface element that is exposed to direct solar radiation. This type of ray is one-time-reflected radiation. Such rays are shown in Figure 3a. The second term represents rays that are reflected once on the spacecraft surface element (which is not exposed to direct solar radiation) and then reach the spacecraft surface element that is exposed to direct solar radiation. This type of ray is twice-reflected radiation, as shown in Figure 3b. The third term represents rays that are reflected twice on the spacecraft surface element (which is not exposed to direct solar radiation) and then reach the spacecraft surface element that is exposed to direct solar radiation. This type of ray is thrice-reflected radiation, as shown in Figure 3c. The  $n$ th term represents rays that are reflected  $n-1$  times on the spacecraft surface element (which is not exposed to direct solar radiation) before reaching the spacecraft surface element that is exposed to direct solar radiation. This type of ray is  $n$ -time-reflected radiation.

$$q_{si}^i = \frac{1}{N_{si}} \left\{ \begin{aligned} & \sum_{j_1=1}^{N_{si}^{A1}} \frac{q_{sd,j_1}}{\alpha^{s,j_1}} \times \alpha_{E_i}^s \times K_1^{si,j_1} + \sum_{j_2=1}^{N_{si}^{A2}} \frac{q_{sd,j_2}}{\alpha^{s,j_2}} \times \alpha_{E_i}^s \times K_2^{si,j_2} \\ & + \dots + \sum_{j_n=1}^{N_{si}^{An}} \frac{q_{sd,j_n}}{\alpha^{s,j_n}} \times \alpha_{E_i}^s \times K_n^{si,j_n} \end{aligned} \right\} \quad (6)$$

where  $K_1^{si,j_1} = \rho_{E_{1,1}}^{s_{j_1}}$ ,  $K_2^{si,j_2} = \rho_{E_{1,2}}^{s_{j_2}} \times \rho_{E_{2,2}}^{s_{j_2}} \dots$ ,  $K_n^{si,j_n} = \prod_{\tau=1}^{n-1} \rho_{E_{\tau,n}}^{s_{j_n}}$ , with  $\rho_{E_{\tau,n}}^{s_{j_n}}$  being the reflectance of the solar spectrum for the face element of the  $\tau$ th intersection of the  $j_n$ th ray in the  $n$ th term of the corresponding expansion.

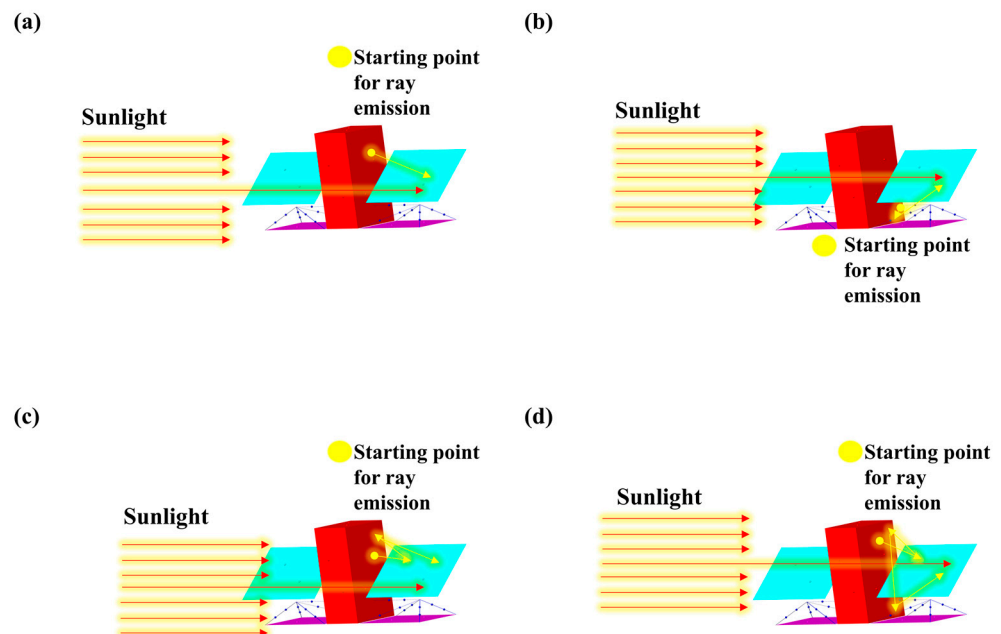


**Figure 3.** Detailed breakdown of the rays counted in the calculation for external heat flux of indirect solar radiation (assuming  $n = 4$ , only the light blue solar panel surface element hit by the red arrow is exposed to direct solar radiation) (a) One-time-reflected radiation external heat flux statistics rays; (b) Twice-reflected radiation external heat flux statistics rays; (c) Thrice-reflected radiation external heat flux statistics rays; (d) Four-time-reflected radiation external heat flux statistics rays.

The face element  $E_i$  emits a total of  $N_{si}$  rays. Of these,  $N_{si}^{A_1}$  rays reach the spacecraft surface element directly exposed to direct solar radiation. There are  $N_{si}^{A_2}$  rays that are reflected once and reach the spacecraft surface element exposed to direct solar radiation. There are  $N_{si}^{A_n}$  rays that are reflected  $n-1$  times and reach the spacecraft surface element exposed to direct solar radiation.  $N_{si}^{A_1}, N_{si}^{A_2}, \dots, N_{si}^{A_n}$  satisfy Equation (7).

$$N_{si}^{A_1} + N_{si}^{A_2} + \dots + N_{si}^{A_n} \leq N_{si} \tag{7}$$

To facilitate the operation, Equation (6) is split into matrix multiplication form. The equation is  $q_{si-old}^i = \frac{1}{N_{si}} \times C_{si} \times D_{si}$ . Suppose  $n = 3$  to illustrate the matrix element composition. At this time, the external heat flux of indirect solar radiation consists of one-time-reflected radiation external heat flux, twice-reflected radiation external heat flux, and thrice-reflected radiation external heat flux.

The  $D_{si}$  matrix is the combined solar spectral reflectance matrix of the spacecraft's face element coating.

$$D_{si} = \begin{bmatrix} A_{si}(1,1) \times A_{si}(1,2) \times A_{si}(1,3) \\ A_{si}(2,1) \times A_{si}(2,2) \times A_{si}(2,3) \\ \vdots \\ A_{si}(n_{si}^m,1) \times A_{si}(n_{si}^m,2) \times A_{si}(n_{si}^m,3) \end{bmatrix}_{n_{si}^m \times 1} \tag{8}$$

The element composition of the  $A_{si}$  matrix is shown in Equation (10).

$$C_{si} = \left[ \begin{array}{c} \frac{q_{sd,1}}{\alpha^{s,1}} \alpha_{E_i}^s, \dots, \frac{q_{sd,N_{si}^{A_1}}}{\alpha^{s,N_{si}^{A_1}}} \alpha_{E_i}^s, \frac{q_{sd,1}}{\alpha^{s,1}} \alpha_{E_i}^s, \dots, \\ \frac{q_{sd,N_{si}^{A_2}}}{\alpha^{s,N_{si}^{A_2}}} \alpha_{E_i}^s, \frac{q_{sd,1}}{\alpha^{s,1}} \alpha_{E_i}^s, \dots, \frac{q_{sd,N_{si}^{A_3}}}{\alpha^{s,N_{si}^{A_3}}} \alpha_{E_i}^s \end{array} \right]_{1 \times n_{si}^m} \tag{9}$$

where  $n_{si}^m = N_{si}^{A_1} + N_{si}^{A_2} + \dots + N_{si}^{A_n}$ . For  $n = 3$ ,  $n_{si}^m = N_{si}^{A_1} + N_{si}^{A_2} + N_{si}^{A_3}$ .

$$A_{si} = \begin{bmatrix} \rho_{E_{1,1}}^{s_1} & 1 & 1 \\ \vdots & \vdots & \vdots \\ \rho_{E_{1,1}}^{s_{N_{si}^{A_1}}} & 1 & 1 \\ \rho_{E_{1,2}}^{s_1} & \rho_{E_{2,2}}^{s_1} & 1 \\ \vdots & \vdots & \vdots \\ \rho_{E_{1,2}}^{s_{N_{si}^{A_2}}} & \rho_{E_{2,2}}^{s_{N_{si}^{A_2}}} & 1 \\ \rho_{E_{1,3}}^{s_1} & \rho_{E_{2,3}}^{s_1} & \rho_{E_{3,3}}^{s_1} \\ \vdots & \vdots & \vdots \\ \rho_{E_{1,3}}^{s_{N_{si}^{A_3}}} & \rho_{E_{2,3}}^{s_{N_{si}^{A_3}}} & \rho_{E_{3,3}}^{s_{N_{si}^{A_3}}} \end{bmatrix}_{(N_{si}^{A_1} + N_{si}^{A_2} + N_{si}^{A_3}) \times 3} \tag{10}$$

The  $A_{si}$  matrix consists of the solar spectral reflectance of the spacecraft's face element coating, described as follows: The first  $N_{si}^{A_1}$  rows of the  $A_{si}$  matrix correspond to the coefficients  $K_1^{si_j_1}$  of the first term of Equation (6). The first column of the matrix is the reflectance of the solar spectrum for the face element where the rays intersect for the first time, and the second and third columns are 1. Rows  $N_{si}^{A_1} + 1$  to  $N_{si}^{A_1} + N_{si}^{A_2}$  correspond to the coefficient  $K_2^{si_j_2}$  of the second term of Equation (6). The first column of the matrix

shows the reflectance of the solar spectrum for the face element where the rays intersect for the first time. The second column shows the reflectance of the solar spectrum for the face element where the rays intersect for the second time. The third column is 1. Rows  $N_{si}^{A1} + N_{si}^{A2} + 1$  to  $N_{si}^{A1} + N_{si}^{A2} + N_{si}^{A3}$  correspond to the coefficient  $K_3^{si/3}$  of the third term of Equation (6). The corresponding first column shows the reflectance of the solar spectrum for the face element where the rays intersect for the first time. The second column shows the reflectance of the solar spectrum for the face element where the rays intersect for the second time. The third column shows the reflectance of the solar spectrum for the face element where the rays intersect for the third time.

$$H_{si} = \begin{bmatrix} \alpha_{E1,1}^{s1} & 0 & 0 \\ \vdots & \vdots & \vdots \\ s_{N_{si}^{A1}} & & \\ \alpha_{E1,1} & 0 & 0 \\ \alpha_{E1,2}^{s1} & \alpha_{E2,2}^{s1} & 0 \\ \vdots & \vdots & \vdots \\ s_{N_{si}^{A2}} & s_{N_{si}^{A2}} & \\ \alpha_{E1,2} & \alpha_{E2,2} & 0 \\ \alpha_{E1,3}^{s1} & \alpha_{E2,3}^{s1} & \alpha_{E3,3}^{s1} \\ \vdots & \vdots & \vdots \\ s_{N_{si}^{A3}} & s_{N_{si}^{A3}} & s_{N_{si}^{A3}} \\ \alpha_{E1,3} & \alpha_{E2,3} & \alpha_{E3,3} \end{bmatrix}_{(N_{si}^{A1} + N_{si}^{A2} + N_{si}^{A3}) \times 3} \tag{11}$$

According to  $\alpha + \rho = 1$ , the elements in the  $A_{si}$  matrix are obtained from the  $H_{si}$  matrix. The elements in  $H_{si}$  are the solar absorption rates of the corresponding surface elements.

### 3.2.2. External Heat Flux of Indirect Solar Radiation Uncertainty Analysis

Before performing the uncertainty analysis, the external heat flux of indirect solar radiation must be calculated once using the RMC method. During this calculation, the number of the intersecting face elements and the solar absorbance of the intersecting face elements need to be recorded for each ray emitted by the target face element of the spacecraft. They are summarized by the intersecting surface element-numbering matrix  $I_{si}$  and matrix  $H_{si}$ , respectively. The spacecraft surface element where the ray finally arrives is recorded. The external heat flux of direct solar radiation  $q_{sd}$  and the solar absorption rate  $\alpha^s$  are recorded for this surface element. Finally, the matrix  $C_{si}$  is generated.

When performing the uncertainty analysis of the external heat flux of indirect solar radiation, ray tracing is no longer performed for each operating condition as in the conventional method. Instead, samples of coated solar absorbance are generated using random numbers. The  $C_{si}$  matrix is updated to the  $C_{si}^1$  matrix based on samples. The  $H_{si}$  matrix is updated to the  $H_{si}^1$  matrix based on the  $I_{si}$  matrix. The  $A_{si}^1$  matrix is calculated using the  $H_{si}^1$  matrix. The  $A_{si}^1$  matrix is used to obtain the  $D_{si}^1$  matrix. Finally, by substituting the resulting matrix into Equation (13), the external heat flux of indirect solar radiation considering uncertainty can be found.

$$D_{si}^1 = \begin{bmatrix} A_{si}^1(1,1) \times A_{si}^1(1,2) \times A_{si}^1(1,3) \\ A_{si}^1(2,1) \times A_{si}^1(2,2) \times A_{si}^1(2,3) \\ \vdots \\ A_{si}^1(n_{si}^m,1) \times A_{si}^1(n_{si}^m,2) \times A_{si}^1(n_{si}^m,3) \end{bmatrix}_{n_{si}^m \times 1} \tag{12}$$

$$q_{si\text{-new}}^i = \frac{1}{N_{si}} \times C_{si}^1 \times D_{si}^1 \tag{13}$$

Note that the elements of each row of the above matrices  $I_{si}$ ,  $H_{si}$ ,  $A_{si}$ , and  $D_{si}$  can be switched in any order. The elements of the columns of matrix  $C_{si}$  can be switched in any order. For ease of presentation, the elements of the matrix in this paper are arranged as follows: In the actual programming calculation, the elements of each row of matrices  $I_{si}$ ,  $H_{si}$ ,  $A_{si}$ , and  $D_{si}$ , as well as the elements of each column of matrix  $C_{si}$ , are directly generated according to the order of the rays emitted by the spacecraft face element. The specific calculation flow chart is shown in Figure 4.

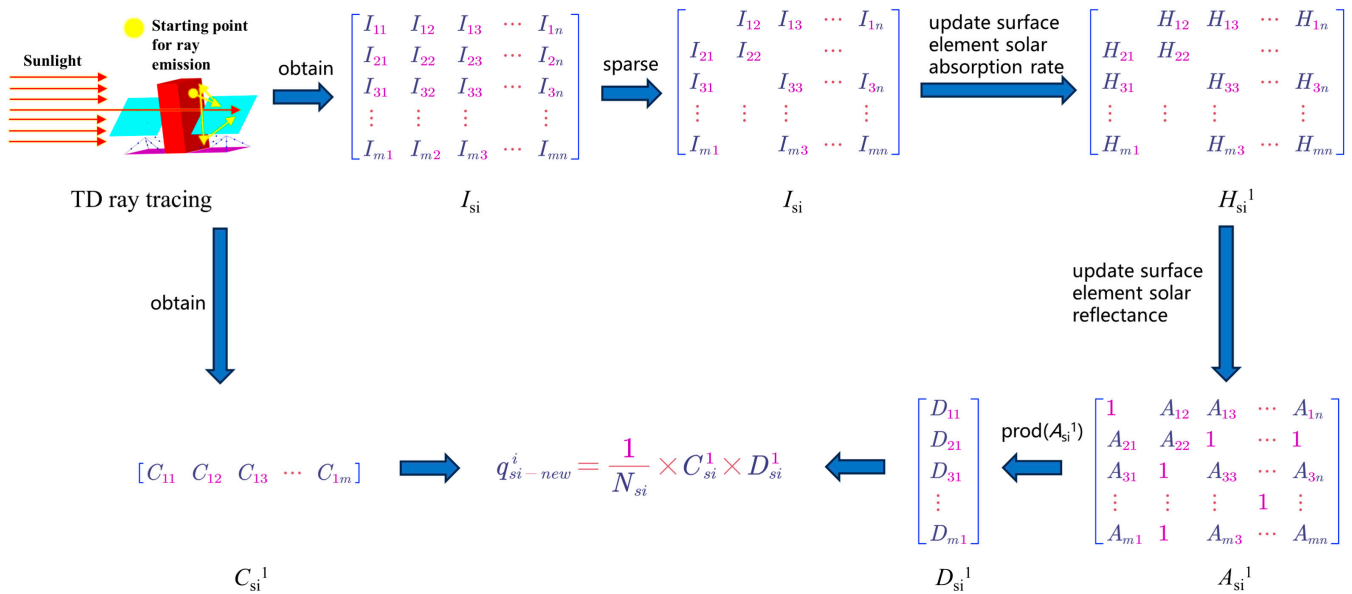


Figure 4. Indirect solar radiation EHFE calculation flow diagram.

The comparison of two processes for calculating the external heat flux of indirect solar radiation taking into account parameter uncertainties is shown in Figure 5.

The main process for calculating the external heat flux of indirect solar radiation considering uncertainties using the conventional method is as follows:

- (1) Samples of solar absorbance and reflectance for all face elements of the spacecraft are generated using random numbers;
- (2) RMC ray tracing is performed to calculate the external heat flux of indirect solar radiation;
- (3) Steps (1) and (2) are repeated to generate multiple  $q_{si}^i$  samples for statistics.

The main process for calculating the external heat flux of indirect solar radiation considering uncertainties using the EHFE formula is as follows:

- (1) RMC ray tracing is performed to solve for the external heat flux of indirect solar radiation. In addition, the  $I_{si}$ ,  $H_{si}$ , and  $C_{si}$  matrices are obtained;
- (2) Samples of solar absorbance and reflectance for all face elements of the spacecraft are generated using random numbers;
- (3) Based on the new solar absorbance sample and the intersecting surface element-numbering matrix  $I_{si}$ , the corresponding elements of matrices  $A_{si}$ ,  $H_{si}$ , and  $C_{si}$  are updated. Matrices  $A_{si}^1$ ,  $H_{si}^1$ , and  $C_{si}^1$  are generated considering the uncertainty parameters. Matrix  $A_{si}^1$  is used to obtain matrix  $D_{si}^1$ ;
- (4) Equation (13) is used to solve for  $q_{si}^{i-new}$ ;
- (5) Steps (2)–(4) are repeated to generate multiple  $q_{si}^{i-new}$  samples for statistics.

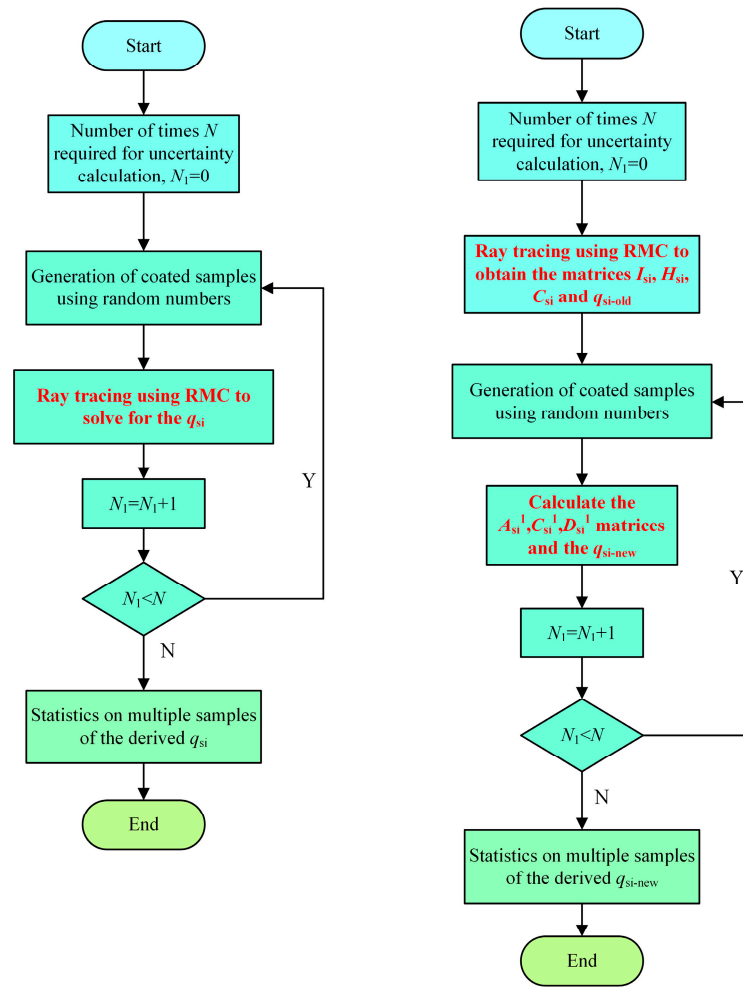


**Figure 5.** Comparison of two processes for solving external heat flux of indirect solar radiation considering parameter uncertainty, left (conventional) and right (based on EHFE equation).

In summary, the original solution to the external heat flux of indirect solar radiation equation is expanded. Then, uncertain variables in the equation are separated, and a new solution formula for the external heat flux of indirect solar radiation is constructed:  $q_{si-old}^i = \frac{1}{N_{si}} \times C_{si} \times D_{si}$ . Based on this formula for thermal uncertainty analysis, ray tracing is performed for only one operating condition; the other operating conditions do not need to emit rays for the complex ray-tracing process. For other operating conditions, the new solar absorptance and reflectance samples are substituted into  $q_{si-new}^i = \frac{1}{N_{si}} \times C_{si}^1 \times D_{si}^1$ . Matrix operations are performed. Using simple matrix operations instead of traditional complex ray-tracing methods can effectively reduce the cost of thermal uncertainty analysis calculations.

**4. Validation Model**

To substantiate the precision and computational efficiency of the solar radiation EHFE formula method, we utilize the spacecraft thermal analysis model depicted in Figure 6 as an example in this study. This model is employed for computations of uncertainty in the orbital external heat flux of solar radiation. Thermal Desktop (TD), the current industry-standard software for spacecraft thermal analysis, was used to construct this model. The model incorporates the satellite body, solar panels, antennae, and trusses. The spacecraft model was discretized into 40 triangular surface elements for the thermal analysis. The numerals affixed to the spacecraft surface elements correspond to those utilized in the ensuing experimental analysis. The external heat flux impacts only the outer surface of this spacecraft; hence, the internal structure of the spacecraft is not contemplated in this

investigation. The orbital and attitude parameters of the spacecraft are recorded in Table 1. As per Figure 6, the spacecraft is discretized into many surface elements, with a given surface of the spacecraft comprised of both a front and a back face element. In this study, we posit that the temperature difference between these two surfaces is marginal, thereby enabling the front and back face elements to share the same numeral. Since the external heat flux inside the satellite body is zero, the satellite body’s back surface element is not considered in this study.

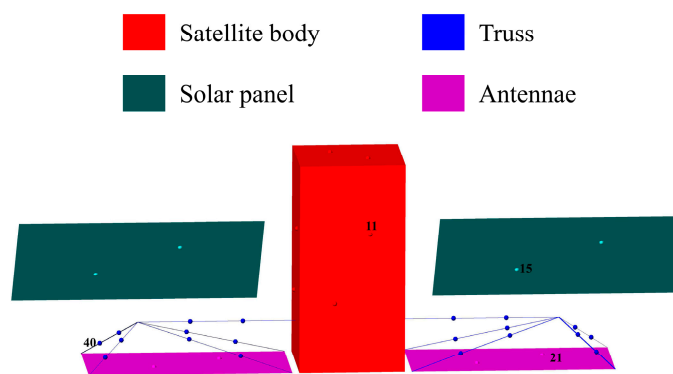


Figure 6. Spacecraft thermal analysis model.

Table 1. Orbital and attitude parameters.

Parameters	Numerical Value
Semimajor axis/(km)	6878
Eccentricity	0
Orbit inclination/(°)	0
Attitude	Z-axis to ground orientation

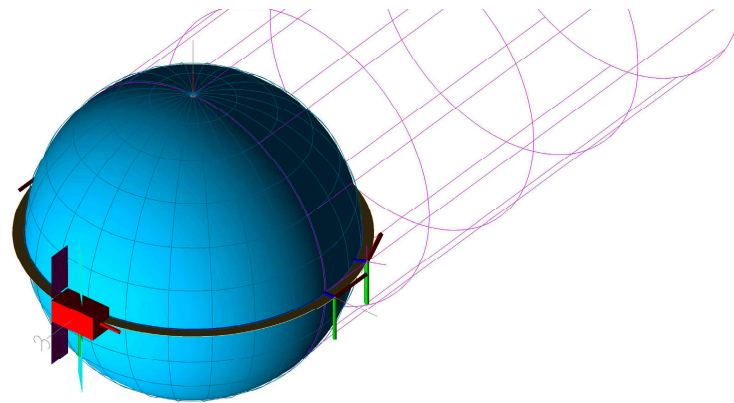
The uncertainty input parameters of interest, along with their average values [26], are depicted in Table 2. The input parameters are normally distributed and their standard deviation is 0.05. One face element each from the spacecraft solar panels, antennae, satellite body, and truss structure are selected as the objects of study. The corresponding face element numerals and their associated components are recorded in Table 3. The initial positioning of the spacecraft, as depicted in Figure 7, situates it within the sunlit sector. At this position, uncertainty analysis of the external heat flux of solar radiation is executed, employing both the conventional method of TD and the solar radiation EHFE formula algorithm. Thereafter, the precision and efficacy of the solar radiation EHFE equation are verified and scrutinized.

Table 2. Average value of the uncertainty variables.

Input Parameters	Average Value
Satellite body solar absorption rate	0.46
Antennae solar absorption rate	0.65
Solar panel solar absorption rate	0.41
Truss solar absorption rate	0.56

Table 3. Spacecraft experimental analysis surface element numbers and their components.

Number of Surface Elements	Spacecraft Components Belonging to Surface Elements
11	Satellite body
15	Solar panel
21	Antennae
40	Truss



**Figure 7.** Spacecraft position of TD at the starting moment.

For the initial external heat flux of solar radiation ray-tracing condition, the values of the solar absorptance of each spacecraft component's coating for this condition are the mean values of the uncertainty variables depicted in Table 2. In calculating the external heat flux of direct solar radiation, the satellite body surface element emits  $1 \times 10^6$  rays, and the other structural surface elements emit  $2 \times 10^6$  rays. In calculating the external heat flux of indirect solar radiation, the satellite body surface element emits  $1 \times 10^6$  rays, and the other structural surface elements emit  $2 \times 10^6$  rays. The matrices  $I_{si}$ ,  $C_{si}$ , and  $D_{si}$  corresponding to the solar radiation EHFE equation are generated from the results of this initial external heat flux ray-tracing condition. Matrices  $C_{si}^1$  and  $D_{si}^1$ , which correspond to the remaining uncertainty conditions, are generated from the matrices  $I_{si}$ ,  $C_{si}$ , and  $D_{si}$  and the samples of solar absorptance relative to the newly imposed conditions. A complex ray-tracing process is not needed here.

Accurately estimating uncertainty bounds for the external heat flux of solar radiation and corresponding confidence intervals of the output response requires precise calculations of the external heat flux response at both ends of its probability density function. According to the referenced literature [7], ensuring that the achieved  $P_{0.95}$  falls within the true  $P_{0.94}$  and  $P_{0.96}$  with a confidence level of 95% requires a minimum of 1900 model iterations. The corresponding solution formula is presented as follows:

$$N_{\min} = P(1 - P) \left( \frac{N_{\sigma}}{\Delta P} \right)^2 \quad (14)$$

where  $N_{\min}$  is the minimum number of runs the model should run,  $P$  is the percentile to be calculated,  $\Delta P$  is the allowable deviation from that value, and  $N_{\sigma}$  is the confidence level that the expected calculated percentile  $P$  lies at the actual  $P - \Delta P$  and  $P + \Delta P$ .

As such, both the traditional TD model and the solar radiation EHFE equation model are executed 2000 times each in this research. This number of iterations provides statistical information corresponding to the anticipated uncertainty in the external heat flux of solar radiation. The analysis is carried out on a computing system equipped with a 3.50 GHz W-2265 CPU and 64 GB of RAM.

## 5. Results and Discussion

The mean, standard deviation, probability density distribution, and confidence interval (CI) of the output response are critical outcomes of interest in uncertainty analysis. To evaluate whether the solar radiation EHFE equation can be substituted for the conventional ray-tracing method, the statistical outcomes of these model output responses over a span of 2000 iterations must be scrutinized and compared.

### 5.1. External Heat Flux of Solar Radiation Uncertainty Analysis

In this study, both the TD model and the EHFE formula were executed 2000 times. Figure 8 depicts the results of these two disparate methods employed for evaluating the

external heat flux of solar radiation pertaining to spacecraft thermal analysis through split-edge violin plots. Quartiles are indicated by blue dashed lines, segmenting the statistical results of each method. The median is indicated by the red dashed line, while the confidence interval extending from the 1st to the 99th percentile is denoted by the pink dashed line. Furthermore, the magnitude of probability density for a particular datum is represented by the contour effect within the violin plots. A more pronounced contour implies a higher probability density associated with the statistical data of that specific point.

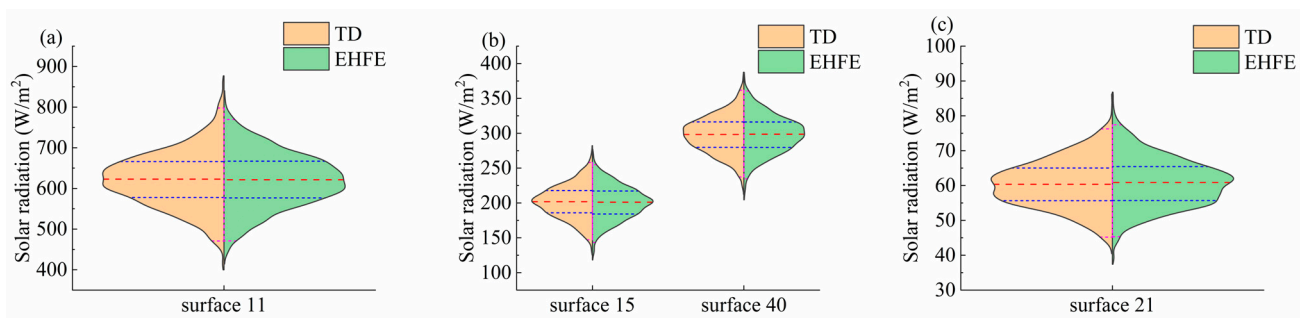


**Figure 8.** Split-edge violin plots of surface elements absorbing external heat flux of solar radiation.

Upon careful examination of the four split-edge violin plots, a conspicuous resemblance is detected between the quartiles, medians, and confidence intervals (extending from the 1st to the 99th percentile) of the statistical data yielded by both the TD and EHFE methodologies. Moreover, the contours within the violin plots representing these two techniques are nearly identical.

Grounded in the qualitative comparison of the split-edge violin plots, the discerned congruity between the outcomes further suggests that the inherent processes and performance indicators of the TD and EHFE methodologies display similar traits. The subsequent discussion includes a thorough quantitative assessment of the statistical results.

The mean quantities, standard deviations, and errors pertaining to the external heat flux of solar radiation assimilated by spacecraft components are depicted in Table 4. The maximum relative discrepancy between the two models is 2.209%, corresponding to the standard deviation of surface element 40. The absolute discrepancy between the models is merely  $0.585 \text{ W/m}^2$ . Upon considering both relative and absolute errors, the margin of error is regarded as tolerable. The relative errors of the average quantities of the external heat flux of solar radiation collected for each surface element fall below 1%. The numerical simulation outcomes regarding the uncertainty of the solar radiation EHFE equation and the TD ray-tracing model are robustly similar.

**Table 4.** Mean and standard deviation of the absorbed external heat flux of solar radiation for the two models of surface elements.

	TD Model ( $\text{W/m}^2$ )	EHFE Equation ( $\text{W/m}^2$ )	Relative Error (%)	Absolute Error ( $\text{W/m}^2$ )
Surface element 11 mean	622.52	620.71	0.292	1.817
Surface element 11 standard deviation	67.59	66.28	1.937	1.309
Surface element 15 mean	201.64	200.44	0.597	1.205
Surface element 15 standard deviation	24.10	24.12	0.076	0.018
Surface element 21 mean	60.51	60.82	0.515	0.312
Surface element 21 standard deviation	6.86	6.94	1.228	0.084
Surface element 40 mean	298.11	298.38	0.092	0.273
Surface element 40 standard deviation	26.47	27.05	2.209	0.585

Figure 9 shows the probability distribution of the external heat flux of solar radiation absorbed by four surface elements of the spacecraft. Meticulously examining these distributions reveals minor differences at the tail and head ends of the probability distribution curves drawn from both the TD model's and the EHFE model's uncertainty calculations, whereas the other portions of the distribution essentially coincide. The results at the 95.4% and 99.7% confidence intervals can be extrapolated from the curves depicted in Figure 7. The selected intervals correspond to  $2\sigma$  and  $3\sigma$  of the normal distribution, respectively. These values typically serve as a benchmark in uncertainty analysis for risk assessment. The comparative results are depicted in Table 5, illustrating a maximum relative discrepancy between the two models of 6.19%. This discrepancy is attributed to surface element 40 at the lower extremity of the 99.7% confidence interval, with an absolute error of  $13.79 \text{ W/m}^2$ .

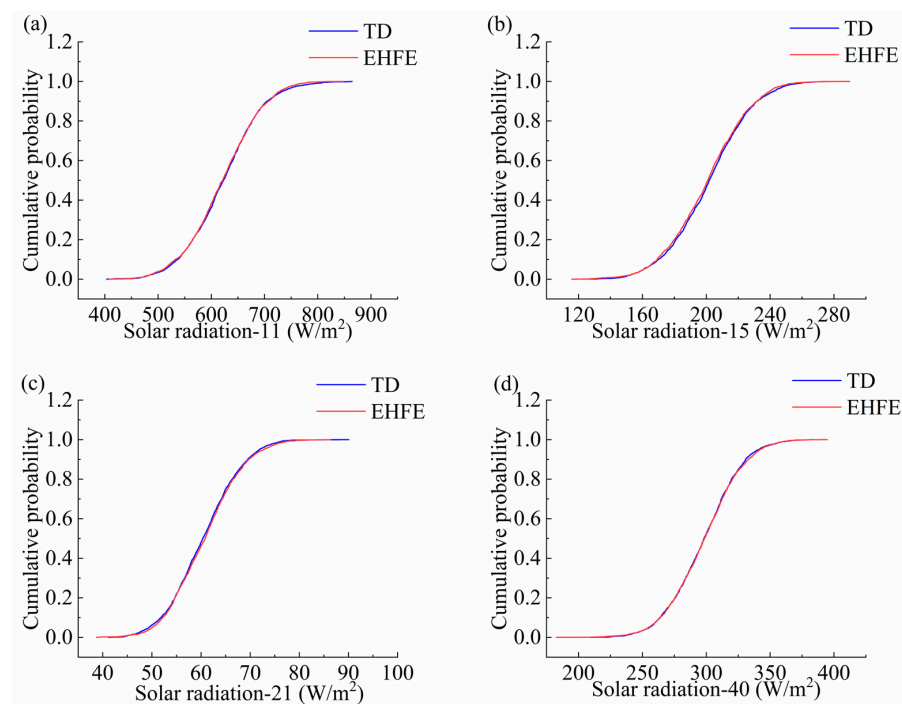
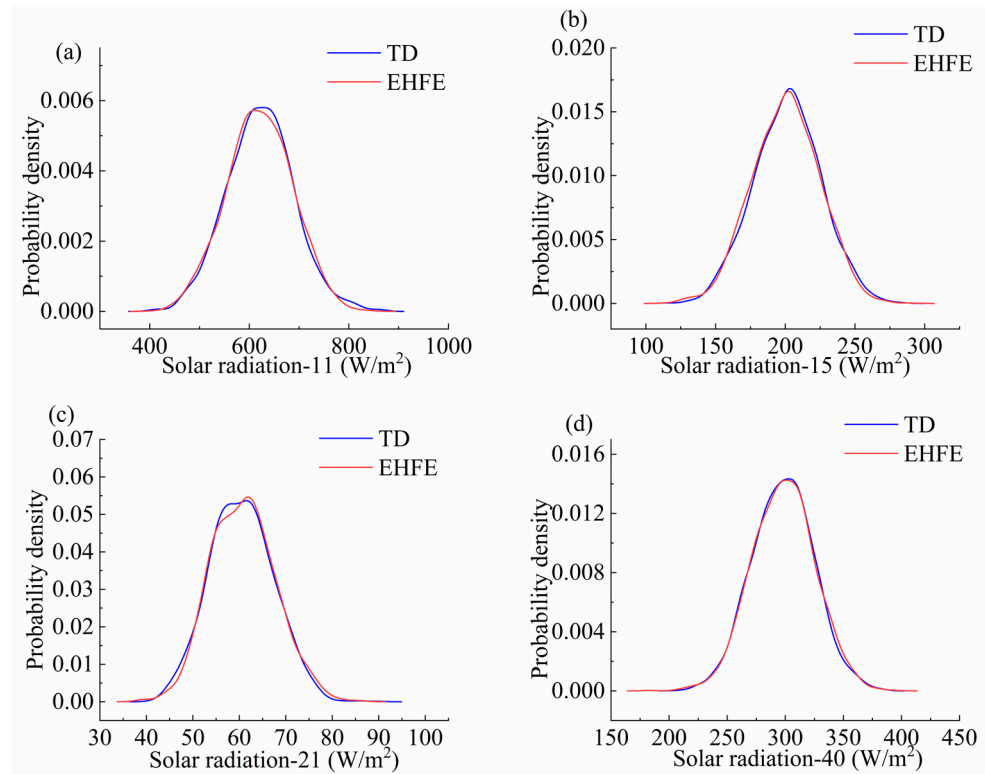


Figure 9. Probability distribution of the surface elements absorbing external heat flux of solar radiation.

Table 5. CI of the external heat flux of solar radiation for both models.

		TD Model (W/m <sup>2</sup> )	EHFE Equation (W/m <sup>2</sup> )	Relative Error (%)	Absolute Error (W/m <sup>2</sup> )
95.40%	Lower CI for surface element 11	486.90	485.53	0.28	1.37
	Upper CI for surface element 11	761.07	749.66	1.50	11.41
	Lower CI for surface element 15	153.11	152.85	0.17	0.26
	Upper CI for surface element 15	249.57	247.04	1.01	2.53
	Lower CI for surface element 21	47.24	47.86	1.30	0.62
	Upper CI for surface element 21	74.27	75.25	1.32	0.98
	Lower CI for surface element 40	244.71	245.02	0.13	0.31
	Upper CI for surface element 40	352.54	352.23	0.09	0.30
99.70%	Lower CI for surface element 11	414.55	435.39	5.03	20.85
	Upper CI for surface element 11	852.90	811.77	4.82	41.13
	Lower CI for surface element 15	131.81	127.23	3.47	4.57
	Upper CI for surface element 15	271.61	271.02	0.22	0.59
	Lower CI for surface element 21	43.03	40.38	6.16	2.65
	Upper CI for surface element 21	82.66	82.79	0.16	0.13
	Lower CI for surface element 40	222.89	209.10	6.19	13.79
	Upper CI for surface element 40	377.96	378.81	0.23	0.86

Figure 10 shows the probability density diagram of the external heat flux of solar radiation absorbed by four surface elements of the spacecraft. Examining the probability density functions procured from the two models for all face elements reveals an overarching concordance, with the curves exhibiting a smooth profile. However, a small deviation between the results of the two models occurs at the highest point, and there is a small difference between the head and tail of the probability density function. Analysis shows that the probability density function yielded from the EHFE equation model effectively approximates the probability density function derived from the TD ray-tracing model for external heat flux calculations.



**Figure 10.** Probability density plots of the surface elements absorbing external heat flux of solar radiation.

The time required to perform 2000 uncertainty analyses for each method is presented in Table 6. The calculation using the solar radiation EHFE formula for the uncertainty analysis of the external heat flux of solar radiation is approximately 17 times faster than that of the TD ray-tracing method. TD-based ray tracing requires the entire CPU capacity for uncertainty analysis of the external heat flux of solar radiation. Conversely, the EHFE-based calculations of external heat flux utilize approximately 80% of the CPU capacity. Thus, the EHFE method demonstrates commendable results without fully utilizing the CPU resources of the computer.

**Table 6.** Time required for the calculation of the uncertainty analysis of external heat flux of solar radiation for each method.

Uncertainty in External Heat Flux of Solar Radiation	
TD(s)	13,020
EHFE equation (s)	753
Speed multiplier (multiple)	17

5.2. Discussion

During the execution of uncertainty analysis in spacecraft thermal management, ray tracing must be repetitively conducted to compute the external heat flux of solar radiation

due to alterations in the thermal property parameters of the spacecraft's surface coating. This process requires  $N$  repetitions and is computationally expensive. Within this study, the formula to calculate the external heat flux of solar radiation absorbed by surface elements is exhaustively expanded. Uncertainty parameters within the formula are segregated and encapsulated into a discrete matrix. For the thermal uncertainty analysis, substituting samples generated by the new operational conditions into the corresponding parameter terms of the matrix is sufficient, negating the requirement for ray tracing.

In the proposed novel method, ray tracing for a singular operational condition is required to calculate the external heat flux of solar radiation and obtain the expanded matrix. The remaining uncertain operational conditions replace the complex ray-tracing process with straightforward matrix operations, contributing substantially to the enhanced computational speed of the proposed method.

The  $H_{si}$  matrix and the intersecting face element-numbering  $I_{si}$  matrix demonstrate a high sparsity ratio, aligning with the properties of sparse matrices. Techniques specific to sparse matrices facilitate initial solar radiation heat flux calculations during ray tracing, yielding  $H_{si}$  and  $I_{si}$  matrices. These methodologies also contribute to updating the  $H_{si}^{-1}$  matrix during the computation of uncertainty in external heat flux. Adopting sparse matrix strategies enables significant memory savings in computational systems and further enhances the computation speed of uncertainty analyses of the external heat flux of solar radiation [27].

When applying the solar radiation EHFE formula for uncertainty analysis, the mean value, standard deviation, and probability functions of the absorbed external heat flux by surface elements align well with those of the TD ray-tracing model. However, discrepancies between the two models emerge, particularly in the upper and lower confidence interval results. Notably, the lower confidence interval of 99.7% for face element 40 substantially deviates from that of the TD ray-tracing model. Several factors, which we explore below, contribute to this discrepancy.

In calculations involving uncertainty in external heat fluxes of solar radiation, the EHFE formula algorithm averts new ray emission under novel working conditions. Nevertheless, its computation matrix is derived based on the tracing of rays emanated in external heat flux calculations under the initial working condition. When new operational circumstances are introduced, parameters pertaining to the thermal properties of the spacecraft's surface coating are altered. During ray propagation, the ray path of the initial working condition is retained without altering the propagation path, despite the likelihood of changes in the energy propagated along this path. When utilizing EHFE for new condition computations, the ray propagation path from the original condition is retained rather than the path from the new TD ray-tracing condition being adopted. Comparing the two paths reveals elongation and truncation of the ray path employed by EHFE, indicating an incorrect truncation point for the ray [28]. This discrepancy underscores the difference between the outcomes derived from the solar radiation EHFE equation and the TD ray-tracing external heat flux calculation model employed in this study.

As illustrated in Figure 11, under initial operational conditions, an incident ray is sequentially reflected off of surface 1 and surface 2 before concluding its trajectory at surface 3. The methodology of uncertainty analysis mandates the consideration of solar absorbance variations in the coatings of surfaces 1, 2, and 3. Such variations inevitably introduce changes in the energy content along the ray's propagation path.

In the scenario presented in Figure 12, the energy  $Q_2$  reflected from surface 3 surpasses a certain threshold, symbolized as  $kQ$ . When this condition holds true, the ray persists in its propagation. As compared to the initial operational state, this results in a more extended ray path.

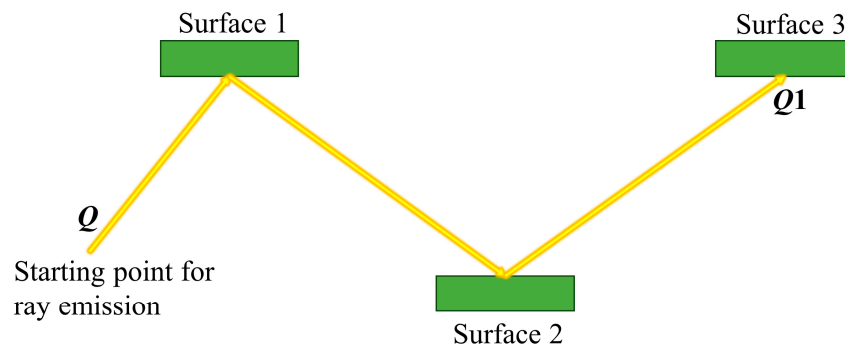


Figure 11. The ray’s propagation path under initial operational condition.

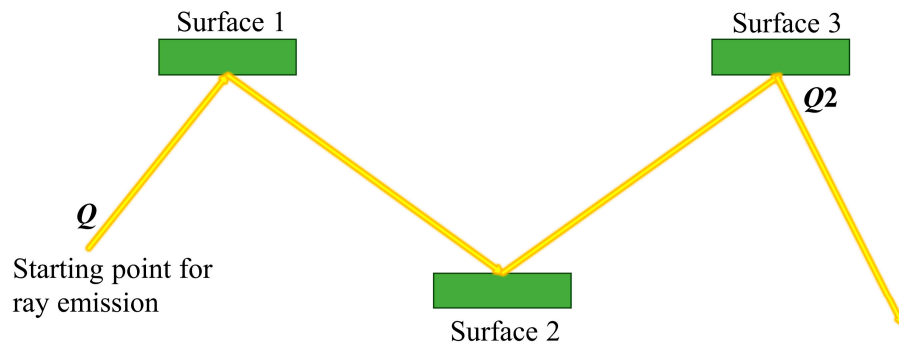


Figure 12. Extended ray path.

Figure 13 depicts an instance where the reflected energy  $Q_3$  from surface 2 is less than or equal to  $kQ$ . Under this condition, the ray discontinues propagation. Compared to the initial operational condition, this results in a shortened ray path.

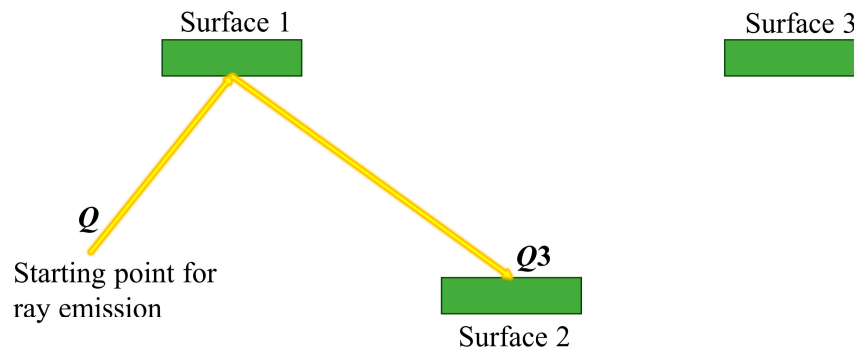


Figure 13. Shortened ray path.

The propagation pathway utilized in EHFE aligns with the trajectory derived from the initial operational conditions. Owing to the inherent uncertainties associated with surface coatings, the propagation pathways under these initial conditions may either elongate or contract relative to the actual operational conditions. This discrepancy constitutes a significant source of error in the uncertainty analysis. Nevertheless, this error can be dynamically mitigated by adjusting the cutoff factor value. Specifically, a smaller cutoff factor corresponds to a reduced error magnitude.

The matrices  $I_{si}$ ,  $C_{si}$ , and  $D_{si}$  from the solar radiation heat flux expansion equations are derived from samples of spacecraft component coatings’ solar absorbance means. In uncertainty analysis, a closer match between solar absorbance samples and mean absorbances of the coatings reduces the error in calculations of the external heat flux of solar radiation of the two models. Given that the solar absorbance sample corresponding to the 99.7% confidence interval substantially deviates from the mean sample, the discrepancy

between the external heat flux of solar radiation estimations generated by the two models is likely substantial. However, this error effect can be attenuated by reducing the value of the cutoff factor.

To enhance the precision of EHFE calculations, the cutoff factor is adjusted from 0.1 to 0.01 and 0.001, keeping other variables constant. Subsequently, the solar radiation heat flux expansion matrix is reconstructed, facilitating the execution of uncertainty calculations for the external heat flux of solar radiation under both the revamped matrix and the TD ray-tracing models. The lower bounds of the 99.7% confidence interval for surface element 40, as calculated by the two methods, are illustrated in Table 7. Reducing the cutoff factor leads to a noticeable decrease in the discrepancy between the results of the two models, demonstrating that the value of the cutoff factor substantially influences the precision of uncertainty analysis based on the solar radiation EHFE formula. However, minimizing the cutoff factor results in extended computation time in external heat flux uncertainty calculations for both models, as indicated in Table 8. Consequently, the value of the cutoff factor must be carefully considered when constructing the solar radiation EHFE matrix.

**Table 7.** Comparison of the calculated lower confidence intervals for 99.7% of the external heat flux of solar radiation absorbed by surface element 40 for different cutoff factors.

	TD Model (W/m <sup>2</sup> )	EHFE Equation (W/m <sup>2</sup> )	Relative Error (%)	Absolute Error (W/m <sup>2</sup> )
Cutoff factor 0.1				
Lower CI for Surface Element 40	222.89	209.10	6.19	13.79
Cutoff factor 0.01				
Lower CI for Surface Element 40	222.83	227.24	1.98	4.41
Cutoff factor 0.001				
Lower CI for Surface Element 40	222.82	219.08	1.68	3.74

**Table 8.** Time required to calculate the uncertainty in external heat flux of solar radiation with different cutoff factors for each method.

	Cutoff Factor 0.01 Uncertainty in External Heat Flux of Solar Radiation	Cutoff Factor 0.001 Uncertainty in External Heat Flux of Solar Radiation
TD (s)	13,190	13,380
EHFE equation (s)	943	1102
Speed multiplier (multiple)	14	12

Furthermore, when performing uncertainty analysis calculations for external heat flux, the coating's solar absorptivity, ray emission points, and ray emission directions are generated as samples based on random number seeds. The differences in these samples between the two models also contribute to the occurrence of random errors.

The analysis of the accuracy and efficiency of the uncertainty in external heat flux of solar radiation calculations carried out by the solar radiation EHFE formula is shown above. Thermal uncertainty analysis calculations conducted using the TD model require ray tracing for each of the  $N$  operational states, which is highly time-consuming. The methodology presented in this paper calls for ray tracing for a singular working condition. An unfolding matrix is created based on this condition and subsequently updated for the remaining conditions to derive the external heat flux of solar radiation for the corresponding circumstances. This approach exhibits significant computational efficiency. Moreover, the error introduced when compared with the TD model can be dynamically calibrated to suit the computational precision aligning with the magnitude of the cutoff factor.

## 6. Conclusions

In this study, the elements of the conventional computation formula for the external heat flux of solar radiation are thoroughly expanded. Uncertainty variable parameters embedded in the formula are distinctly segregated, and the formula is transmuted into a form resembling the product of two matrices. Consequently, a novel equation for calculating the external heat flux of solar radiation is formed.

The solar radiation EHFE formula requires ray tracing for only one of the  $N$  operating conditions of the uncertainty calculations for the external heat of solar radiation. The external heat flux is computed utilizing this particular condition as a foundation, and the corresponding matrix for the expansion equation is constructed. The subsequent operating conditions remove the need for ray tracing. Instead, new uncertainty samples are directly incorporated into the appropriate slots within the matrix. Subsequently, matrix manipulations are conducted to derive the uncertainty in the external heat flux of solar radiation.

The solar radiation EHFE equation supplants the intricate and computationally demanding ray-tracing procedure with a straightforward matrix operation. Additionally, the computational matrix embedded in the EHFE equation exhibits a substantial sparsity ratio. Integrating sparse matrix storage and computational strategies within external heat flux uncertainty computations yields considerable computational efficiency.

The uncertainty calculation for the external heat flux of solar radiation was executed on a specific spacecraft as a case study. The mean value, standard deviation, probability distribution function, confidence interval, probability density function, and computation duration, among other outcomes, were identified. These outcomes demonstrate that the computational precision of the solar radiation EHFE equation is akin to that of the conventional TD external heat flux of solar radiation calculation results, albeit with a markedly diminished computation time.

In the uncertainty analysis, the maximum relative discrepancy between the two models for the mean and standard deviation of the external heat flux of solar radiation was found to be 2.209%. For the upper and lower confidence interval bounds, the maximum relative discrepancy reached 6.19%. However, the discrepancy can be reduced by adjusting the cutoff factor in the EHFE model. When the cutoff factor was decreased from 0.1 to 0.001, the relative discrepancy dropped from 6.19% down to 1.68%. This demonstrates that tuning the cutoff factor provides a mechanism to enhance the precision of the EHFE model results relative to the TD benchmark.

The matrix necessary for the solar radiation EHFE equation is derived via the path length method approach to ray tracing, incorporating a cutoff factor. Including the cutoff factor prompts a lengthening and shortening of the ray propagation path, resulting in discrepancies with conventional ray-tracing computations for the external heat flux of solar radiation. Nevertheless, the user is able to alter the magnitude of the cutoff factor, thereby dynamically adjusting the computational accuracy.

The solar radiation EHFE equation proposed herein can be broadly generalized.  $S$  in the calculation formula for the external heat flux of solar radiation in this paper is the solar constant. The solar constant is the solar radiation intensity at the mean Sun–Earth distance. To estimate the external heat flux of solar radiation at other orbital locations throughout the solar system, the uncertainty in the external heat flux of solar radiation at a given position can be obtained by directly replacing the solar constant in the equation with the solar radiation intensity here. This expanded equation provides a valuable reference for enhancing the efficacy of spacecraft thermal analysis computations, particularly those involving uncertainties. Furthermore, this study lays groundwork for addressing uncertainties inherent in the thermal design of future deep space exploration vehicles, solar observational satellites, and space solar power stations.

**Author Contributions:** Conceptualization, X.F.; methodology, L.L., W.M., H.C., Y.Z. and X.F.; software, L.L. and X.F.; validation, L.L. and X.F.; formal analysis, L.L., W.M., H.C. and X.F.; investigation, L.L. and X.F.; data curation, L.L., W.M. and X.F.; writing—original draft, L.L., W.M. and X.F.; writing—review and editing, Y.Z., L.L., W.M., H.C. and X.F. All authors have read and agreed to the published version of the manuscript.

**Funding:** This research received no external funding.

**Data Availability Statement:** The data presented in this study are available upon request from the corresponding author.

**Conflicts of Interest:** The authors declare no conflict of interest.

## Nomenclature

$S$	the solar constant ( $W/m^2$ )
$E_i$	node $i$ surface element
$q_{sd}^i$	external heat flux of direct solar radiation absorbed by the face element $E_i$ ( $W/m^2$ )
$q_{si}^i$	external heat flux of indirect solar radiation absorbed by the face element $E_i$ ( $W/m^2$ )
$q_s^i$	external heat flux of solar radiation absorbed by the face element $E_i$ ( $W/m^2$ )
$D_{si}$	the combined solar spectral reflectance matrix of the spacecraft face element coating
$I_{si}$	the intersecting face number matrix
$H_{si}$	solar absorbance matrix of intersecting surface elements from $I_{si}$
$A_{si}$	solar spectral reflectance matrix of intersecting surface elements from $I_{si}$
$C_{si}$	the multiplication of each common factor of the EHFE formula by $q_{sd,j}/\alpha^{s,j}$
$N_{min}$	the minimum number of model runs
$N_\sigma$	number of standard deviations
$P$	percentile
$\Delta P$	deviation from percentile
Greek symbols	
$\alpha_{E_i}^s$	the solar absorption rate of surface element $i$
$\rho_{E_{\tau,n}}^{s_{jn}}$	the reflectance of the solar spectrum for the face element of the $\tau$ th intersection of the $j_n$ th ray
$\alpha$	the surface solar absorption rate
$\rho$	the surface solar reflectance
$\theta$	the angle between the normal vector of the face element $E_i$ and the solar ray vector (deg)
Subscripts/Superscripts	
$i$	current node
$j$	node other than current
Acronyms	
MC	Monte Carlo
RMC	Reverse Monte Carlo
EHFE	external heat flux expansion
TD	Thermal Desktop
CI	confidence interval

## References

1. Kuzenov, V.V.; Ryzhkov, S.V.; Varaksin, A.Y. Calculation of heat transfer and drag coefficients for aircraft geometric models. *Appl. Sci.* **2022**, *12*, 11011. [\[CrossRef\]](#)
2. Fagherazzi, M.; Santi, M.; Barato, F.; Pizzarelli, M. A Simplified Thermal Analysis Model for Regeneratively Cooled Rocket Engine Thrust Chambers and Its Calibration with Experimental Data. *Aerospace* **2023**, *10*, 403. [\[CrossRef\]](#)
3. Ishimoto, T.; Bevans, J.T. Temperature variance in spacecraft thermal analysis. *J. Spacecr. Rockets* **1968**, *5*, 1372–1376. [\[CrossRef\]](#)
4. Howell, J.R. Monte Carlo treatment of data uncertainties in thermal analysis. *J. Spacecr. Rockets* **1973**, *10*, 411–414. [\[CrossRef\]](#)
5. Thunnissen, D.P.; Tsuyuki, G.T. Margin determination in the design and development of a thermal control system. *SAE Trans.* **2004**, *113*, 899–916.

6. Thunnissen, D.P.; Au, S.K.; Tsuyuki, G.T. Uncertainty quantification in estimating critical spacecraft component temperatures. *J. Thermophys. Heat Transf.* **2007**, *21*, 422–430. [[CrossRef](#)]
7. Gómez-San-Juan, A.; Pérez-Grande, I.; Sanz-Andrés, A. Uncertainty calculation for spacecraft thermal models using a generalized SEA method. *Acta Astronaut.* **2018**, *151*, 691–702. [[CrossRef](#)]
8. Xiong, Y.; Guo, L.; Yang, Y.; Wang, H. Intelligent sensitivity analysis framework based on machine learning for spacecraft thermal design. *Aerosp. Sci. Technol.* **2021**, *118*, 106927. [[CrossRef](#)]
9. Kato, H.; Ando, M.; Fukuzoe, M. Toward Uncertainty Quantification in Satellite Thermal Design. *Trans. Jpn. Soc. Aeronaut. Space Sci. Aerosp. Technol. Jpn.* **2019**, *17*, 134–141. [[CrossRef](#)]
10. Regis, R.G. Evolutionary programming for high-dimensional constrained expensive black-box optimization using radial basis functions. *IEEE Trans. Evol. Comput.* **2013**, *18*, 326–347. [[CrossRef](#)]
11. Kleijnen, J.P. Kriging metamodeling in simulation: A review. *Eur. J. Oper. Res.* **2009**, *192*, 707–716. [[CrossRef](#)]
12. Han, Z.-H.; Zhang, Y.; Song, C.-X.; Zhang, K.-S. Weighted gradient-enhanced kriging for high-dimensional surrogate modeling and design optimization. *AIAA J.* **2017**, *55*, 4330–4346. [[CrossRef](#)]
13. Qian, J.; Yi, J.; Cheng, Y.; Liu, J.; Zhou, Q. A sequential constraints updating approach for Kriging surrogate model-assisted engineering optimization design problem. *Eng. Comput.* **2020**, *36*, 993–1009. [[CrossRef](#)]
14. Datta, R.; Regis, R.G. A surrogate-assisted evolution strategy for constrained multi-objective optimization. *Expert Syst. Appl.* **2016**, *57*, 270–284. [[CrossRef](#)]
15. Song, Z.; Murray, B.T.; Sammakia, B.; Lu, S. Multi-Objective Optimization of Temperature Distributions Using Artificial Neural Networks. In Proceedings of the 13th InterSociety Conference on Thermal and Thermomechanical Phenomena in Electronic Systems, San Diego, CA, USA, 30 May–1 June 2012; pp. 1209–1218.
16. Altan, A.; Aslan, Ö.; Hacıoğlu, R. Real-Time Control Based on NARX Neural Network of Hexarotor UAV with Load Transporting System for Path Tracking. In Proceedings of the 2018 6th International Conference on Control Engineering & Information Technology (CEIT), Istanbul, Turkey, 25–27 October 2018; pp. 1–6.
17. Kromanis, R.; Kripakaran, P. Support vector regression for anomaly detection from measurement histories. *Adv. Eng. Inform.* **2013**, *27*, 486–495. [[CrossRef](#)]
18. Rahmani, S.; Ebrahimi, M.; Honaramooz, A. A surrogate-based optimization using polynomial response surface in collaboration with population-based evolutionary algorithm. In *Advances in Structural and Multidisciplinary Optimization, Proceedings of the 12th World Congress of Structural and Multidisciplinary Optimization (WCSMO12) 12, Braunschweig, Germany, 5–9 June 2017*; Springer: Cham, Switzerland, 2018; pp. 269–280.
19. Kersch, A.; Morokoff, W.; Schuster, A. Radiative heat transfer with quasi-Monte Carlo methods. *Transp. Theor. Stat. Phys.* **1994**, *23*, 1001–1021. [[CrossRef](#)]
20. Liu, Y.; Li, G.-H.; Jiang, L.-X. A new improved solution to thermal network problem in heat-transfer analysis of spacecraft. *Aerosp. Sci. Technol.* **2010**, *14*, 225–234. [[CrossRef](#)]
21. Yuan, M.; Li, Y.-Z.; Sun, Y.; Ye, B. The space quadrant and intelligent occlusion calculation methods for the external heat flux of China space Station. *Appl. Therm. Eng.* **2022**, *212*, 118572. [[CrossRef](#)]
22. Yang, W.; Cheng, H.; Cai, A. Thermal analysis for folded solar array of spacecraft in orbit. *Appl. Therm. Eng.* **2004**, *24*, 595–607. [[CrossRef](#)]
23. Farrahi, A.; Pérez-Grande, I. Simplified analysis of the thermal behavior of a spinning satellite flying over Sun-synchronous orbits. *Appl. Therm. Eng.* **2017**, *125*, 1146–1156. [[CrossRef](#)]
24. Krainova, I.; Nenarokomov, A.; Nikolichev, I.; Titov, D.; Chumakov, V. Radiative Heat Fluxes in Orbital Space Flight. *J. Eng. Thermophys.* **2022**, *31*, 441–457. [[CrossRef](#)]
25. Li, P.; Cheng, H.-E.; Qin, W.-B. Numerical simulation of temperature field in solar arrays of spacecraft in low earth orbit. *Numer. Heat Transf. A Appl.* **2006**, *49*, 803–820. [[CrossRef](#)]
26. Selvadurai, S.; Chandran, A.; Valentini, D.; Lamprecht, B. Passive Thermal Control Design Methods, Analysis, Comparison, and Evaluation for Micro and Nanosatellites Carrying Infrared Imager. *Appl. Sci.* **2022**, *12*, 2858. [[CrossRef](#)]
27. Yang, F.; Li, J.; Xu, C.; Li, D.; Qiu, H.; Xu, A. MPI Parallelization of Numerical Simulations for Pulsed Vacuum Arc Plasma Plumes Based on a Hybrid DSMC/PIC Algorithm. *Aerospace* **2022**, *9*, 538. [[CrossRef](#)]
28. Fu, X.; Hua, Y.; Ma, W.; Cui, H.; Zhao, Y. An Innovative External Heat Flow Expansion Formula for Efficient Uncertainty Analysis in Spacecraft Earth Radiation Heat Flow Calculations. *Aerospace* **2023**, *10*, 605. [[CrossRef](#)]

**Disclaimer/Publisher’s Note:** The statements, opinions and data contained in all publications are solely those of the individual author(s) and contributor(s) and not of MDPI and/or the editor(s). MDPI and/or the editor(s) disclaim responsibility for any injury to people or property resulting from any ideas, methods, instructions or products referred to in the content.